

TABLE 1. Galaxy Parameters^a

Galaxy	Type	Distance ^b (Mpc)	i	V_h (km/s)	l	b
NGC 55	SBm	1.66	90°	140	332.88°	-75.74°
NGC 253	SBc/Sc	2.58	78.5° ^c	249	97.43°	-87.96°
NGC 300	Sd	1.80	46°	145	299.22°	-79.42°

^aFrom Tully (1988), unless otherwise indicated.

^bDistances from Puche & Carignan (1988).

^cThe inclination of NGC 253 is from Pence (1981).

This figure "Hoopes.fig1_2.jpg" is available in "jpg" format from:

<http://arxiv.org/ps/astro-ph/9607048v2>

TABLE 2. Observation Log

Galaxy	Exposure Time			Rms Noise ^a	
	H α	[SII]	Continuum	H α	[SII]
NGC 55	6 \times 600s	6 \times 600s	6 \times 600s	3.1	3.4
NGC 253	6 \times 600s	6 \times 600s	6 \times 600s	2.1	2.1
NGC 300	5 \times 540s	6 \times 540s	6 \times 540s	2.6	2.7

^a $\times 10^{-17}$ ergs s⁻¹ cm⁻² arcsec⁻².

This figure "Hoopes.fig3.jpg" is available in "jpg" format from:

<http://arxiv.org/ps/astro-ph/9607048v2>

TABLE 3. Observed Properties

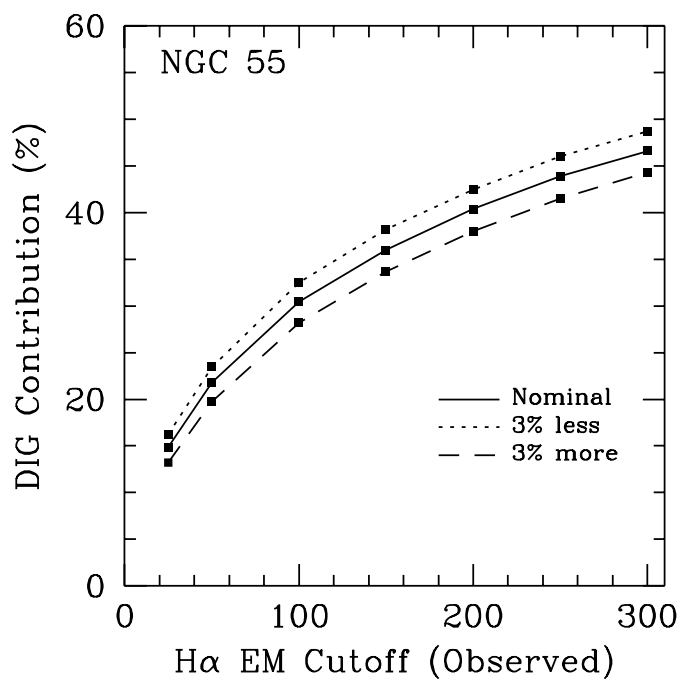
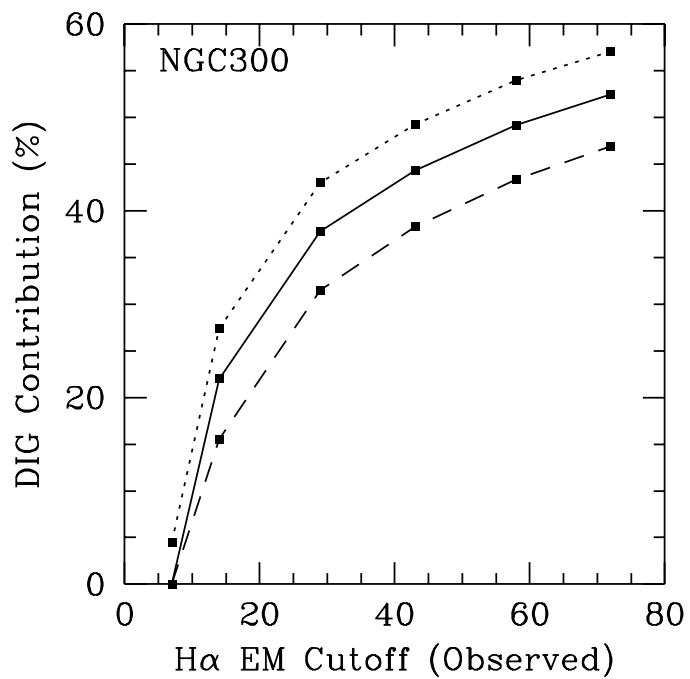
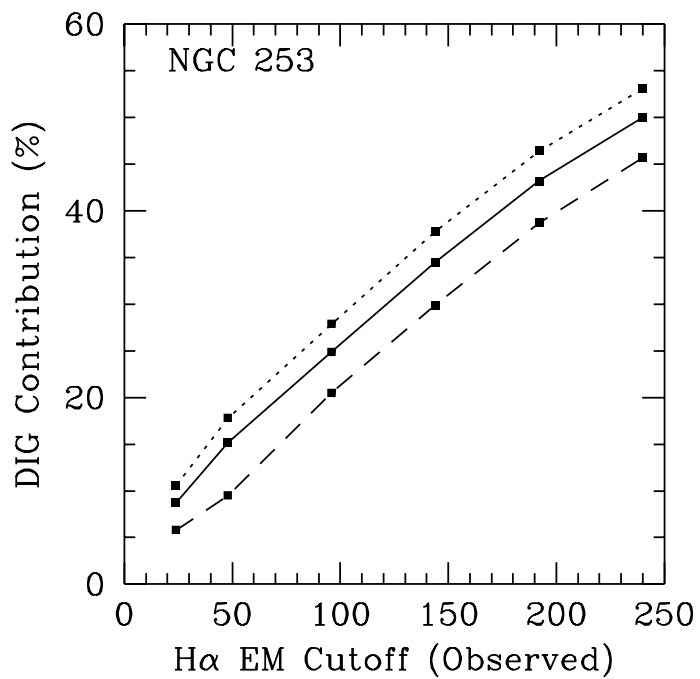
Galaxy	$L_{H\alpha+[NII]}$	Diffuse Fraction		$\frac{[SII]6716+6731\text{\AA}}{H\alpha+[NII]6548+6583\text{\AA}}$ Ratio ^{a,b}		
		Measured	Corrected for Scattering	Global	DIG	HII Regions
NGC 55	$2.6 \times 10^{40} \pm 11\%$	33 – 38%	31 – 35%	0.27 ± 0.06	0.38 ± 0.07	0.21 ± 0.02
NGC 253	$6.2 \times 10^{40} \pm 12\%$	35 – 43%	30 – 36%	0.25 ± 0.14	0.42 ± 0.22	0.21 ± 0.07
NGC 300	$1.4 \times 10^{40} \pm 12\%$	48 – 58%	44 – 54%	0.29 ± 0.11	0.34 ± 0.11	0.24 ± 0.02

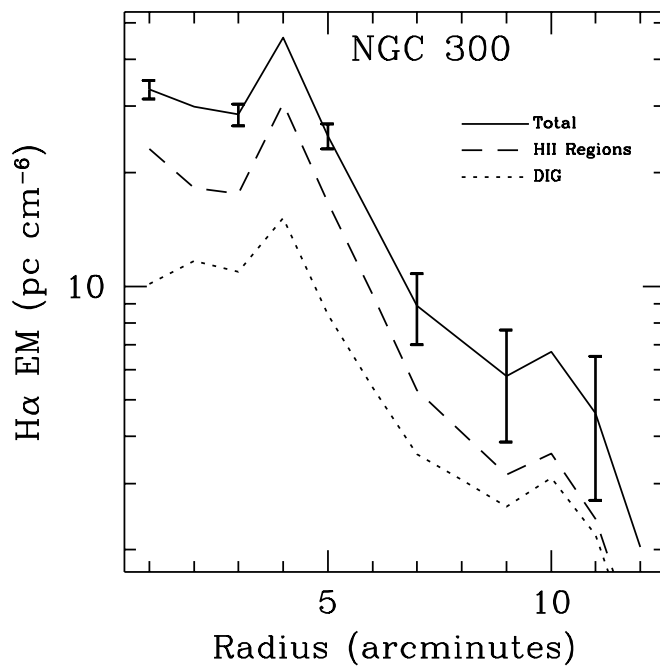
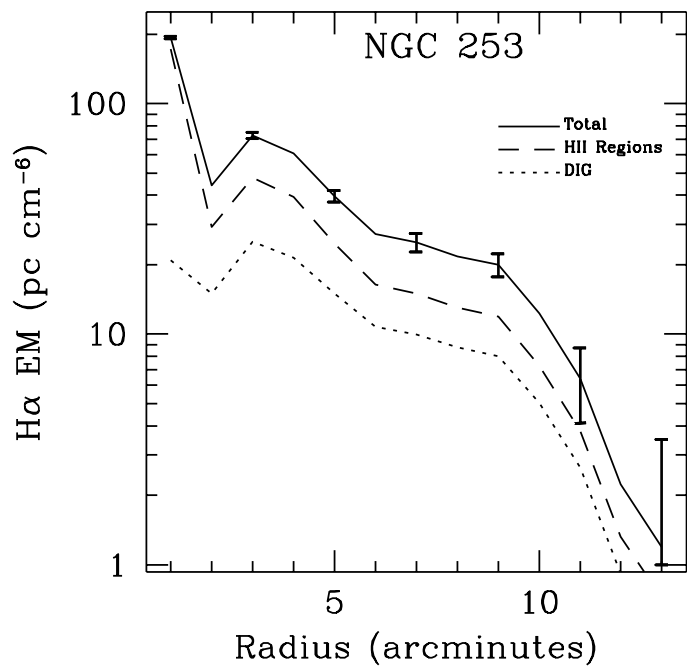
^aThe uncertainties listed for all three ratios are derived from the estimated error in the diffuse fraction. They are correlated in the sense that if the ratio for HII regions were to increase, the ratio for the DIG would also increase. Thus the differences between the DIG and HII region ratios are significant despite the large error bars.

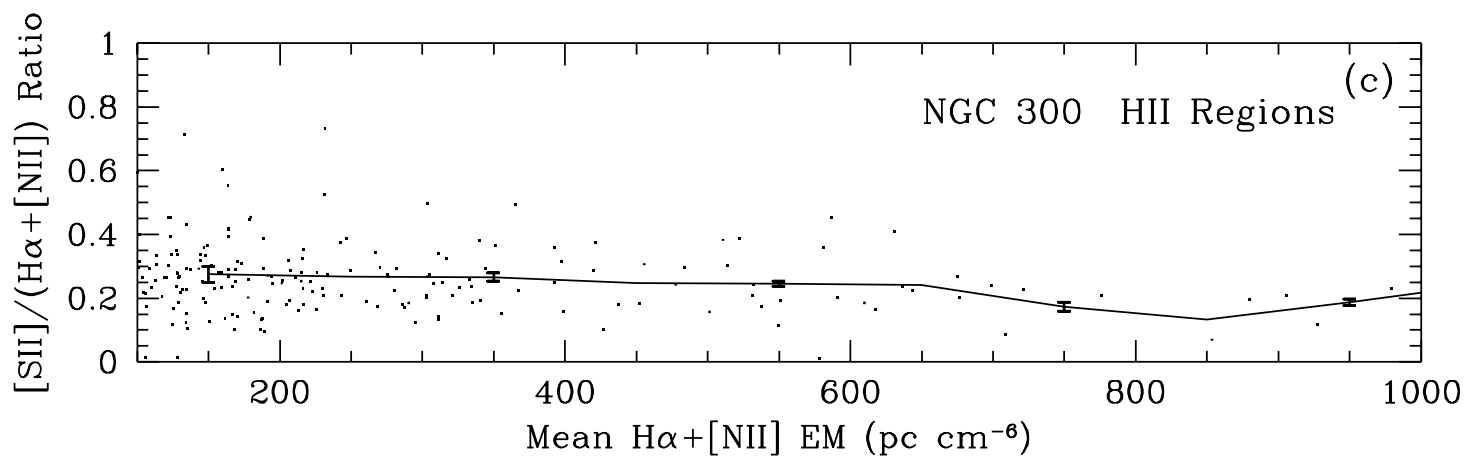
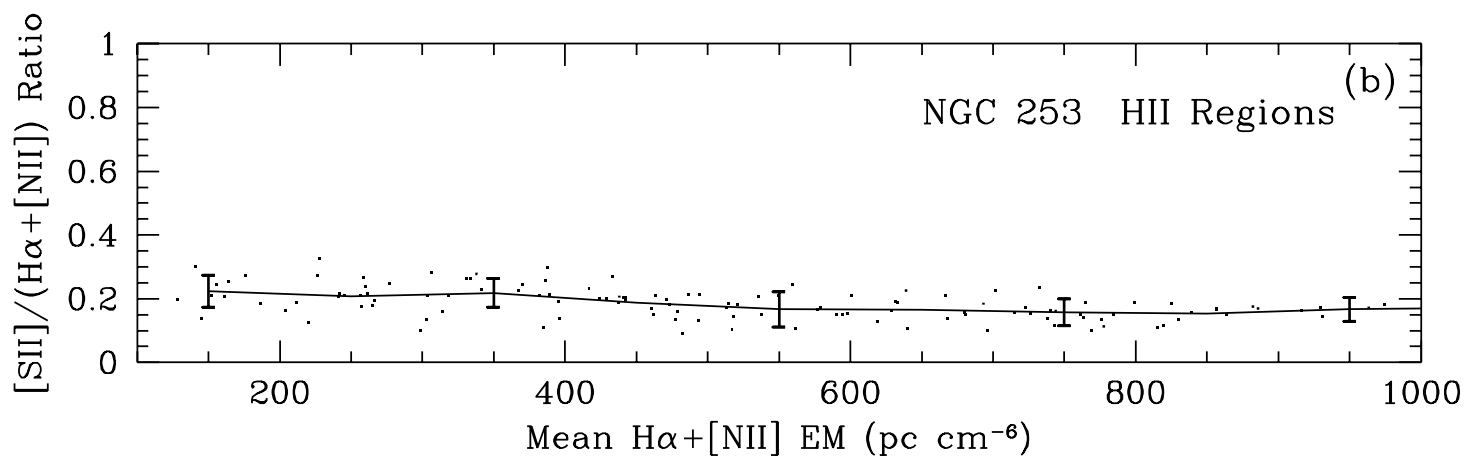
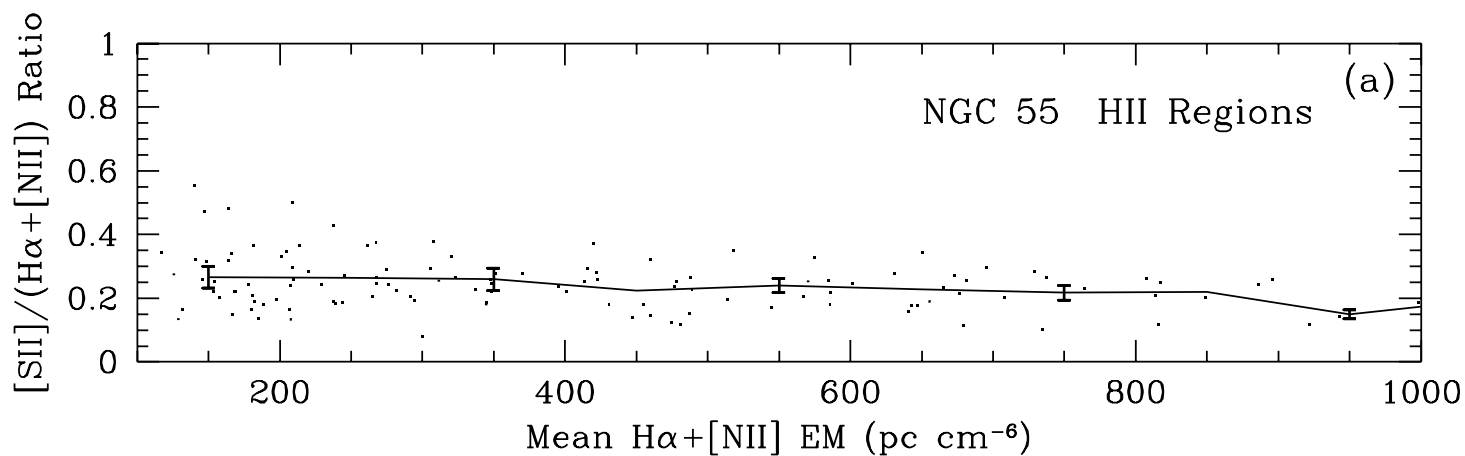
^bCorrected for scattered light.

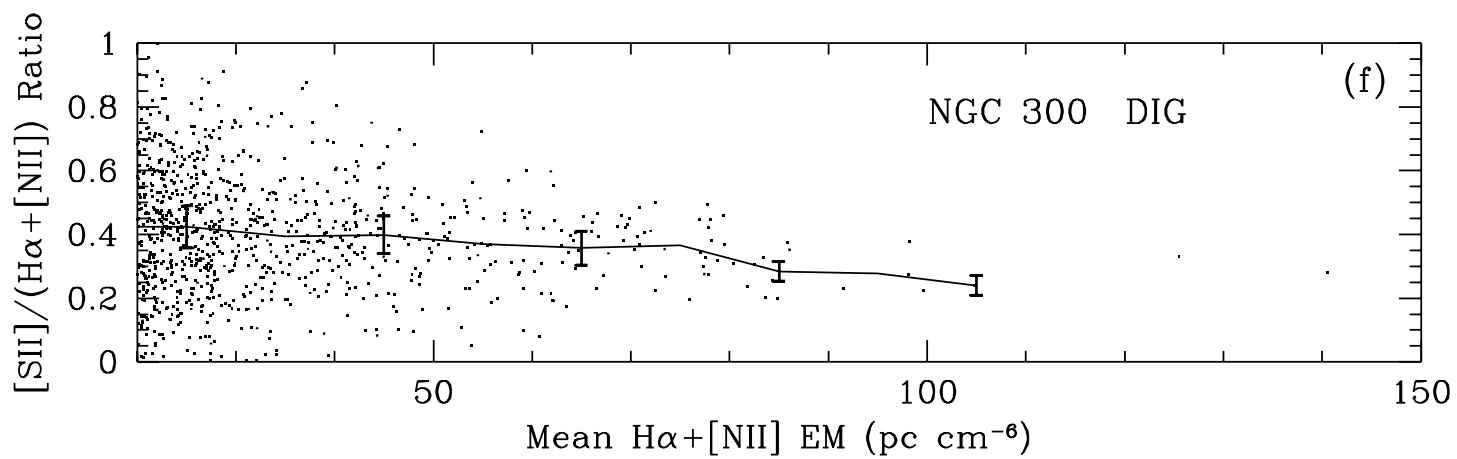
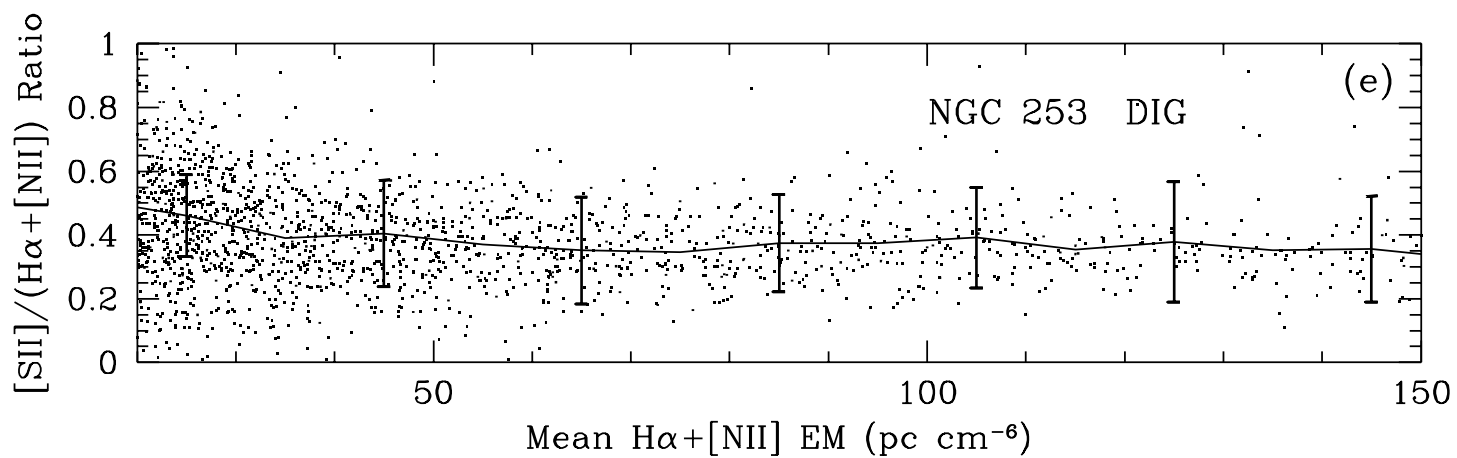
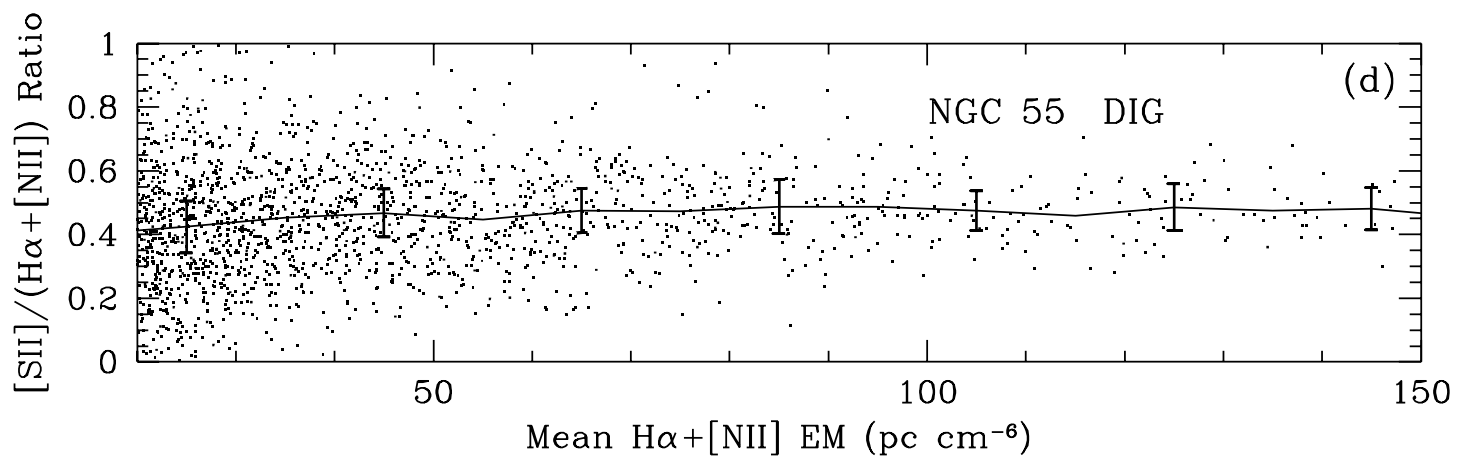
This figure "Hoopes.fig4.jpg" is available in "jpg" format from:

<http://arxiv.org/ps/astro-ph/9607048v2>









To be published in the *Astronomical Journal*

Diffuse Ionized Gas in Three Sculptor Group Galaxies

Charles G. Hoopes, René A. M. Walterbos¹, and Bruce E. Greenawalt
 New Mexico State University, Department of Astronomy, Box 30001/Dept. 4500,
 Las Cruces, New Mexico 88003
 choopes@NMSU.edu, rwalterb@NMSU.edu, bgreenaw@NMSU.edu

ABSTRACT

We present a study of the diffuse ionized gas (DIG) in three Sculptor group galaxies: NGC 55, NGC 253, and NGC 300. The study is based on narrow band imagery in $H\alpha + [NII]$ (6548+6583Å) and $[SII]$ (6717+6731Å). We find that DIG contributes 33 to 58% of the total $H\alpha$ luminosity in these galaxies, or 30 to 54% after correcting for scattered light. We find that NGC 300 has a higher fractional DIG luminosity than the other galaxies in our sample, but it is not clear whether this is a significant difference or an effect of the high inclination of the other galaxies. The diffuse emission, averaged over the optical extent of the disk, has a face-on emission measure of 5 to 10 pc cm⁻⁶. The DIG is concentrated near HII regions, although significant emission is seen at large distances from HII regions, up to 0.5 to 1 kpc. The $[SII]/(H\alpha + [NII])$ ratio is enhanced in the DIG, typically around 0.3 to 0.5, compared to 0.2 for the HII regions in these galaxies. These properties are similar to those measured for the DIG in the Milky Way and in other nearby spirals. The line ratios, large-scale distribution, and energy requirement suggest that photoionization is the dominant ionization mechanism.

Subject headings: Galaxies: Individual (NGC 55, NGC 253, NGC 300) —
 Galaxies: Interstellar Matter — Galaxies: Irregular — Galaxies: Spiral —
 Galaxies: Starburst — ISM: Bubbles

¹Visiting Astronomer, Cerro Tololo Inter-American Observatory. CTIO is operated by AURA, Inc. under cooperative agreement with the National Science Foundation.

1. Introduction

In recent years it has been recognized that a major component of the Galactic interstellar medium is the diffuse ionized gas (DIG, sometimes called the warm ionized medium or WIM). This gas has been studied using several techniques, including pulsar dispersion measurements (*e.g.* Reynolds 1991) and optical line emission (*e.g.* Reynolds 1984, 1988). These observations show the Galactic DIG to be widespread, warm ($T \sim 8000$ K), and diffuse ($n_e \sim 0.2 \text{ cm}^{-3}$). It has a large vertical extent, with a scale height of about 900 pc, fills 20% of the Galactic volume, and accounts for most of the mass of ionized gas (Reynolds 1991). The spectrum of the DIG differs from that of HII regions in several respects. An example that is particularly relevant to this study is the [SII] 6716+6731Å/H α ratio, which is typically about twice as high in the DIG as in HII regions (Reynolds 1985,1988). A large amount of energy, about $10^{42} \text{ ergs s}^{-1}$, is needed to keep this gas ionized, which can only be provided easily by Lyman continuum photons from OB stars, and is just barely met by supernova shocks (Kulkarni & Heiles 1988).

Investigation of the DIG has recently been extended to external galaxies. The vertical extent of the DIG has been studied in several edge-on galaxies, such as NGC 891 (Rand, Kulkarni, & Hester 1990; Dettmar 1990; Keppel *et al.* 1991; Dettmar & Schulz 1992), but few face-on galaxies have been investigated. Detailed studies of non-edge-on systems have been carried out only for M31 (Walterbos & Braun 1994, hereafter WB94, Walterbos & Braun 1992), for NGC 247 and NGC 7793 (Ferguson *et al.* 1996), and for several irregular galaxies (Hunter & Gallagher 1990, 1992). An investigation of the DIG in M51, M81, and several other nearby spirals is currently in progress (Greenawalt & Walterbos 1996). More limited analysis of the DIG has been done for M33 (Hester & Kulkarni 1990) and NGC 2403 (Sivan *et al.* 1990). In the face-on systems that have been studied DIG appears to contribute 30 to 50% of the total H α luminosity. The galaxies that have been observed in [SII] show an enhanced [SII]/H α ratio similar to that observed for the galactic DIG.

Although a general understanding of DIG characteristics is emerging, the relatively small number of galaxies that have been studied makes it difficult to draw universal conclusions, and several questions remain unanswered. The connection of DIG with OB stars and HII regions, and questions such as variation with galaxy type and star-formation rate need to be investigated further to help constrain the ionization mechanism. We present a study of the DIG component of three galaxies in the Sculptor group: NGC 55, NGC 253, and NGC 300. Our project is independent of the recent study by Ferguson *et al.* (1996) of two other Sculptor spirals, NGC 7793 and NGC 247. The mean distance to the Sculptor group is 2.5 Mpc, making these galaxies ideally suited for this type of study. Table 1 presents some of the properties of these galaxies.

In §2 of this paper we outline the observational procedure and data reduction techniques, including tests for scattered light contribution. The morphology of the DIG in the Sculptor galaxies is described in §3. In §4, we calculate the luminosity of the DIG, and in §5 we investigate the spectral characteristics. Finally, §6 contains a summary and discussion of the results.

2. The Data

2.1. Observations and Data Reduction

The data were obtained in September, 1990, with the 0.6 meter Curtis/Schmidt telescope at CTIO. A Thompson 1024x1024 chip was used, providing a field of view of 30.7×30.7 arcmin². The pixel size of this chip is 1."84 when used with the Schmidt. Exposure times were 6×600 seconds in each filter for NGC 253 and NGC 55, and 6×540 seconds for NGC 300. We obtained images in each of three filters: a 68Å wide H α filter, a 91Å wide [SII] 6716+6731Å filter, and a 77Å wide continuum filter centered on 6649Å. The H α filter also contains the contribution from the [NII] 6548Å and 6584Å lines. The spectro-photometric standards LTT 7987 and LTT 9293 were observed as well. NGC 253 and NGC 300 were observed under photometric conditions, but NGC 55 was observed through cirrus. Table 2 is a log of the observations.

We reduced the CCD frames following standard procedures. Dome flats from various nights were co-added to create one “super flat,” which we used to correct for gain variations across the chip. We shifted the images to a common grid, convolved to the worst seeing of the set, and averaged using the *combine* task in IRAF. Cosmic ray events were eliminated using the “ccdclip” option in *combine*. Bad pixels were replaced with the median value of the neighboring pixels. The continuum image was scaled to the line images (see §2.2) and subtracted, producing net emission-line images. Remnants of bright foreground stars were removed manually in IRAF and replaced by the mean of the neighboring pixels. The NGC 253 and NGC 300 images were calibrated using the observed spectrophotometric standards (Hamuy et al. 1992). NGC 55 was taken under non-photometric conditions. We derived a calibration for NGC 55 using the published R-band magnitudes (Alcaino & Liller 1984) of stars in the field.

2.2. Uncertainties

The rms noise in the images, measured on the background, is given in table 2. One must also be concerned about flat fielding errors when working with continuum subtracted images, which can produce variation over large regions in the net line images. By comparing individual flat-field images, we estimate that a 1% flat fielding uncertainty may exist over the region of the chip containing the galaxies. This error is in both the line and continuum images, so when the continuum is subtracted the uncertainty may be compounded. For NGC 253 a 1% error in the flat fielding could produce a systematic uncertainty in the worst case of about 4.6 pc cm^{-6} when comparing one side of the disk to another. For NGC 300 the uncertainty is 3.9 pc cm^{-6} , and 4.6 pc cm^{-6} for NGC 55.

During the observations we experienced problems with horizontal banding structure in the bias level of the CCD. Usually the bands were low-level, on the order of a few counts, but some images contained jumps of tens or hundreds of counts. The NGC 253 and NGC 300 images were corrected satisfactorily with overscan subtraction, but the problem was worse on the night that NGC 55 was observed. We manually removed the large bands from the image, and corrected for the smaller jumps using a higher order fit to the overscan region of the chip. Our efforts substantially increased the quality of the images, but some banding is still evident in the final images. This is the origin of the diagonal pattern in the background of the NGC 55 image (figure 1). The remaining structure is very low level (less than 3 pc cm^{-6} in emission measure). It is obvious in the figure because the image is displayed so that the lowest levels can be seen to emphasize the diffuse emission.

A critical procedure in the data reduction is the continuum subtraction. To determine an initial scale factor with which to multiply the continuum image to scale it to the line images, we measured the fluxes of about 20 stars in the frame of each galaxy in each filter, and calculated the multiplicative factor needed to make the mean of the stellar fluxes in different filters equal. However, the foreground stars do not necessarily reflect the continuum spectrum of the galaxies. We also determined scaling factors by comparing regions in each galaxy which appeared to be free of line emission. This only led to adjustments for NGC 300, where the net $\text{H}\alpha + [\text{NII}]$ image produced using the scale factor from foreground stars became negative in certain regions, while the net $[\text{SII}]$ image still appeared to contain significant continuum emission. Adjusting the scale factor of the continuum image by -2% for $\text{H}\alpha + [\text{NII}]$ image, and by $+6\%$ for the $[\text{SII}]$ (as indicated by the line-free galaxy regions) seemed to produce more plausible results. The scale factor derived from the foreground star would have produced unrealistically high $[\text{SII}]/\text{H}\alpha$ ratios. In view of this, we estimate that the scale factor used in subtracting the continuum may be uncertain at the $\pm 3\%$ level and wherever appropriate we quote the corresponding uncertainties.

The southwest side of NGC 253 (Figure 2) appears weaker in $H\alpha$ than the rest of the galaxy. This is the side that is red-shifted due to rotation, with a maximum redshift of about 5\AA . Combined with the 5\AA systemic redshift of NGC 253, the $H\alpha$ line is then shifted up to 10\AA with respect to the center of our filter. In addition, the F3.5 beam of the Schmidt telescope causes the filter passband to be blue shifted about 10\AA . While $H\alpha$ is still well within the filter, [NII] at 6584\AA is shifted to about the 50% transmission level. The 5\AA rotational redshift of NGC 253 pushes the line further toward the edge of the passband for the southwest side of the galaxy. This may be the cause of the difference in appearance of the two sides of the galaxy, and may affect our determination of the total $H\alpha$ luminosity. Kennicutt (1992) finds an average [NII]/ $H\alpha$ ratio for spiral disks of 0.5. Assuming this is also true for NGC 253, a loss of half of the flux from [NII] 6584 would reduce the observed $H\alpha + [\text{NII}]$ flux by 17% on that side of the disk. It should not affect the other two galaxies, whose systemic velocities produce redshifts of only 3\AA , and whose rotational velocities are much less than that of NGC 253 (Tully 1988).

2.3. Scattered Light

It is crucial to our study of the DIG that we understand the contribution of scattered light. Light scattered by the optics in the telescope and camera produces wings in the point spread function, which might be interpreted as low-level emission surrounding bright objects like stars or HII regions. Emission by HII regions may also be scattered by dust in the galaxy, again producing diffuse emission around HII regions. We tested for these effects following WB94.

We determined the point spread function (PSF) for two bright stars on images in both filters, to see how much of the stellar flux was scattered into the extended tail. The resulting stellar profiles extend over a range of more than $10 \text{ mag arcsec}^{-2}$. In these profiles, 95% of the measured flux from the star is contained within 9 pixels ($16''$) in the $H\alpha$ image, and within 13 pixels ($24''$) in the [SII] image. Light scattered in the telescope would be concentrated within $16''$ of HII regions (in $H\alpha$), and not more than 5% of the total $H\alpha$ flux would come from beyond this radius around HII regions. However, we find that the actual $H\alpha$ contribution of the DIG is substantially larger than this. To test this quantitatively, we made an image of the PSF using unsaturated foreground stars in the images. We convolved the PSF with an image containing only the HII regions, with the DIG masked out, to simulate the scattering of light due to HII regions. We then masked out the HII regions from the convolved image using the method discussed in §4.2, which left only the light scattered out of the HII regions, and compared the scattered light to the diffuse emission

in the original images. As an example, in NGC 253 the contribution of the DIG to the total $H\alpha+[NII]$ emission was reduced from 40% to 33% if the scattered light is removed, indicating that 18% of the diffuse emission is in fact scattered light. The DIG contribution to the total $[SII]$ luminosity drops from 54% to 50%, a reduction of 7%. In NGC 300, the diffuse $H\alpha+[NII]$ emission was reduced by 8% when this correction was made, and the diffuse $[SII]$ emission dropped by 7%. In NGC 55, the $H\alpha+[NII]$ correction was 8%, and the $[SII]$ correction was 6%. We conclude that up to 20% of the DIG flux in $H\alpha$ may in fact be due to scattered light, but only 10% in $[SII]$. The fraction is less in $[SII]$ even though the PSF appears more extended, because the $[SII]$ emission from HII regions is much fainter. We have applied this correction to our measured DIG fractions, but we will also give our results without the correction for comparison with previous studies.

Light scattering by dust in the galaxy as the dominant source of the diffuse emission is unlikely because the $[SII]/H\alpha$ ratio observed in the DIG is quite different from that observed in HII regions. Additionally, light scattered by dust would usually be concentrated around HII regions, but the DIG emission can occur in distinct patches or filaments far from HII regions.

3. Morphology of the DIG

The continuum subtracted $H\alpha$ images of NGC 55, NGC 253, and NGC 300 are shown in figures 1-3. The images are calibrated in emission measure and displayed logarithmically to show the faint emission of the DIG. These images show that diffuse ionized gas is clearly present in these galaxies.

As noted earlier, NGC 253 is a prototypical nuclear starburst. The likely heavily obscured $H\alpha$ luminosity of the nucleus alone is about 6×10^{38} ergs s^{-1} (measured in an 8.1" aperture, which corresponds to a diameter of 63 pc). To the south and east of the nucleus is the outflow cone, powered by stellar winds and supernovae in the starburst nucleus (Schulz & Wegner 1992; Heckman *et al.* 1990 and references). There are many bright HII regions, especially in the central 7 kpc of the galaxy, along the two well-defined spiral arms. Emission from diffuse ionized gas is distributed between the HII regions along the arms, but is strongest close to HII regions. In the outer part of the galaxy the DIG is usually associated with a specific HII region, and in the inner parts where there are many HII regions the DIG is spread throughout the arms and even into the inter-arm region. At the limited resolution of the data, the DIG structure is primarily diffuse, although some filamentary structure can be seen, especially on the northwest edge of the galaxy.

NGC 300 is quiescent in comparison to NGC 253, as shown by the relatively small number of bright HII regions and lower $H\alpha$ luminosity (Table 3). Diffuse emission is again primarily associated with HII regions. Here it can be seen that the morphology is a combination of diffuse and filamentary structures. The filamentary structure of the DIG in NGC 300 is striking. Loops or shells, possibly remnants of expanding shells which were driven by the stellar winds and supernovae of OB associations, dominate the morphology. Some of these loops are associated with star-forming regions, while others are completely isolated from any bright HII regions. Both complete and partial shells are visible.

The continuum subtracted $H\alpha$ image of NGC 55 also shows diffuse and filamentary emission from DIG. Again, the trend is for diffuse emission to be concentrated near star-forming regions, and to decrease in intensity as one moves away from HII regions. DIG is most evident in the central 4 kpc of the galaxy, where the largest HII regions are also seen. This image also shows diffuse emission extending vertically from the plane of the galaxy. On both sides the emission can be traced vertically more than 1.5 kpc from the plane.

The central region and halo of this galaxy shows prominent filamentary structure in the DIG. A large emission-line loop north and east of the nuclear bulge has been observed previously in [OIII] (Graham & Lawrie 1982). This loop is present in our $H\alpha$ image but not in [SII]. The [SII] image has similar noise than the $H\alpha$ image, but the expected signal will be weaker so the loop may be below our limit of detection. The upper limit to the [SII]/ $H\alpha$ + [NII] line ratio is 0.25. We do detect another loop on the south side of the galaxy in both $H\alpha$ and [SII]. This loop is smaller but more obvious than the north loop in our $H\alpha$ image. In addition, more loop- and shell-like structures are seen in $H\alpha$ east of the southern loop, and a large filament extends south of the galaxy on the west side of this southern loop in both filters. This filament can be traced for 1.5 kpc in $H\alpha$. The loops and filaments may be related to stellar wind and supernovae driven shells, similar to those in NGC 300, and indicate a connection of the disk ISM to the halo gas.

In summary, all three galaxies show emission from diffuse ionized gas. The distribution is both filamentary, as in the loops and shells, and a diffuse layer in the inner disks. Qualitatively, there is a correlation between the distribution of DIG and that of HII regions, implying a connection with star formation. In the following sections we will explore this connection in more detail.

4. Luminosity of the DIG

4.1. Total H α Luminosity

The H α + [NII] luminosities of each galaxy were calculated by integrating pixel values over the image. We removed foreground stars from the image and then set the background to zero by subtracting a plane fit to the border of the image. The derived luminosities are given in table 3. These galaxies are located well out of the plane of the Milky Way ($b \leq -75^\circ$), so the correction for foreground extinction is small (Burstein & Heiles 1984), much less than our observational uncertainty. We also did not correct for internal extinction, which could have a significant effect in NGC 253 and NGC 55, but is difficult to quantify.

The uncertainties in table 2 were derived by varying the continuum subtraction by $\pm 3\%$. The luminosity for the nucleus of NGC 253 is 6.3×10^{38} ergs s $^{-1}$, 13% lower than that measured by Keel (1984), including a rough correction for the shifting of the [NII] 6584Å line in the filter. This is the only independent determination of the H α flux from NGC 253 that we found in the literature.

We calculated the star-formation rate (SFR) from the total H α luminosity (Kennicutt 1983), giving about $0.2 M_\odot yr^{-1}$ for NGC 55, $0.4 M_\odot yr^{-1}$ for NGC 253, and $0.1 M_\odot yr^{-1}$ in NGC 300. These values are very uncertain, especially in NGC 253 and NGC 55, due to internal extinction. Although the SFR for NGC 253 derived from the H α luminosity is only a factor of four greater than that of NGC 300, the FIR luminosity (Rice *et al.* 1988) rescaled to our adopted distance gives a $L_{FIR}/L_{H\alpha+[NII]}$ ratio of 178 for NGC 253, but only 15 for NGC 55 and 12 for NGC 300. This discrepancy probably indicates that most of the H α emission in NGC 253 is obscured. High resolution FIR imaging of NGC 253 (Smith & Harvey 1996) show that $\geq 70\%$ of the FIR luminosity arises from the starburst nucleus. The H α emission from the nucleus is likely heavily obscured by dust, and the disk itself is known to be extremely dusty (Sofue *et al.* 1994, Sandage 1961), so it is not surprising that the H α + [NII] luminosity is low compared to the FIR luminosity. The SFR of NGC 253 may be a factor of ten or more higher than that indicated by the H α luminosity. It is clear that these galaxies have widely varying star formation properties.

4.2. Isolating the Diffuse Emission on the Images

Perhaps the most reliable method to estimate the H α flux contributed by the DIG in a galaxy is to subtract from the total H α flux the contribution from discrete HII regions and other emission line sources (e.g., WB94). However, this method requires identification and individual flux measurements, using aperture photometry with correction for local background fluxes, for several hundred to as much as a thousand objects. Given the

difference in the surface brightness of the DIG compared with discrete emission line nebulae, it should be possible to get the desired number in a more straightforward way by masking out discrete sources before summing up the flux. A possible complication, however, which is especially severe in strongly inclined galaxies, is that the discrete source population is superposed on a potentially varying DIG background. This implies that a simple cut at a single surface brightness level (e.g., Ferguson *et al.* 1996) to isolate DIG from HII regions is not a suitable method in all cases. As an example, in Fig. 4a, we show the image of NGC 253 cut an isophotal level of 80 pc cm^{-6} , the level chosen by Ferguson *et al.* for NGC 247 and NGC 7793. The entire inner disk of the galaxy has been clipped, whereas inspection of Fig. 2 shows that DIG is clearly present in this region. Cutting at a higher intensity level results in leaving in too many HII regions in the outer disk.

A related problem is that the DIG intensities are likely to increase with inclination, simply due to projection effects. Cutting all galaxies in the sample at a constant isophotal level would therefore lead to DIG fractions that will have potentially large systematic differences that are mostly the result of the method used to measure the DIG. To circumvent this, we developed a slightly more sophisticated masking technique to isolate the DIG.

The $\text{H}\alpha$ image of each galaxy was median filtered with a large box (90×90 arcseconds) to remove the small structure in the image and leave only the large scale variations. We experimented with different sized boxes on the Sculptor galaxies and on the M31 images of WB94. These images are more sensitive and have better spatial resolution than our Sculptor group images. In WB94 it was therefore possible to calculate an accurate DIG luminosity using the source subtraction technique. We chose the box size that gave diffuse fractions for the M31 fields that were on average consistent with those found in WB94 and applied a box with the corresponding linear size to the Sculptor galaxies. The median filtered image was then subtracted from the original to remove the large scale emission across the galaxy, leaving only the small scale structure. The resulting image was slightly smoothed to reduce the noise. A mask was defined on this image by making a cut at a constant surface brightness level of 50 pc cm^{-6} . Pixels below the limit were replaced with a value of one, and those above were replaced with zero. This mask was then multiplied with the original $\text{H}\alpha$ image, resulting in an image of the DIG component of each galaxy, with pixels in HII regions replaced with zero flux. The pixel values in the masked image were added to get the total emission from the DIG. This was compared to the total $\text{H}\alpha$ luminosity to get the contribution of DIG emission to the total $\text{H}\alpha$ luminosity of each galaxy.

The DIG flux measured from the masked image is an underestimate, because we are neglecting diffuse emission that may be superimposed on the masked HII regions. To correct for this, we estimated the mean intensity of the DIG emission in the galaxy, and multiplied

this with the number of masked pixels. This may still be an underestimate, because the DIG emission near HII regions may well be higher than the mean. We also corrected for the scattered light contribution to the DIG using the method discussed in §2.3.

We found that this method produced diffuse fractions for the inclined galaxies that are relatively insensitive to the cutoff level used on the median-subtracted image. The diffuse fraction for NGC 300 is still somewhat sensitive to the cut level. Our cut at 50 pc cm^{-6} results in a relatively high diffuse fraction of $53 \pm 5\%$. If the cut is made at 30 pc cm^{-6} , the diffuse fraction is $45 \pm 5\%$ for NGC 300. A masked image of NGC 253 made with this method is shown in figure 4b for illustration. This mask is much better at differentiating between the DIG and HII regions in both the faint outer disk and the bright inner disk. Comparison with figure 4a shows that this method works better than a cut at constant surface brightness, especially for inclined galaxies such as NGC 253.

We also investigated whether a large fraction of the DIG luminosity might be contributed by faint unresolved HII regions. To test for this, we estimated the faintest HII regions that could be distinguished from the background and hence masked out of the images. This luminosity limit is about $10^{36} \text{ erg s}^{-1}$ for all three galaxies. Using the HII region luminosity function derived by Kennicutt *et al.* (1989), we estimated the contribution of HII regions below this limit to the DIG flux. The contribution is less than 5% in all three cases.

4.3. The Diffuse Fractions and Mean Emission Measure

The measured diffuse fractions are given in table 3. The range was found by varying the continuum subtraction by $\pm 3\%$. The diffuse fraction measured in NGC 55 and NGC 253 could still be a lower limit, due to the difficulty in isolating DIG from HII regions in inclined galaxies. It is therefore not clear that the somewhat lower fractions in these two systems indicate a real difference with NGC 300. With this in mind, the fraction of $\text{H}\alpha$ luminosity arising in the DIG appears to be remarkably constant, especially given the varied nature of these galaxies. The diffuse fractions measured here are similar to those measured in other nearby galaxies, such as M31 (WB94), M51 and M81 (Greenawalt & Walterbos 1996), and NGC 247 and NGC 7793, two other Sculptor group galaxies (Ferguson, *et al.* 1996).

While we believe that the fractional DIG fluxes measured this way are accurate, we have also derived numbers using a simple cut at a single isophotal level. This showed that the difference in DIG fraction between the galaxies in our sample and that of Ferguson *et al.* (1996) can be easily attributed to the measurement technique. A disadvantage

of the median filter method is that we lose the ability to determine how the DIG flux increases if cuts are made at successively higher intensities. A reason for doing this would be to compare the estimates for the Galaxy, which are based on solar neighborhood data, with external systems. In particular, all external systems looked at so far indicate *higher* fractional Lyman continuum requirements than determined for the Galaxy. However, we believe that this is likely due to the different level of the DIG present in the solar neighborhood compared to the average galaxy disk. In particular, in figure 5 we show how the fractional DIG flux increases as we increase the isophotal cutoff level to mask out the DIG. Our conclusion is that the relatively low estimate (10 to 15%, Reynolds 1991b) of the fraction of Lyman continuum photons required to ionize the DIG in the Galaxy, compared to the results obtained for external systems, is most likely due to the presence of the Sun in a region of rather low DIG surface brightness, with an EM of about 5 to 6 pc cm⁻⁶, while the average values in spiral arms and even across entire disks, are substantially higher (see table 3). If we restrict the DIG in the Sculptor galaxies to face-on EM levels below 6 pc cm⁻⁶ we also find 10 to 15%, rather than 30 to 50%.

The average emission measure in the DIG was determined within the 25th blue magnitude isophote on the inclination corrected disks of NGC 253 and NGC 300. For NGC 253, the average EM in the DIG is 6.1 – 9.7 pc cm⁻⁶. The range in values is the results of varying the continuum subtraction by $\pm 3\%$. The average emission measure for the nominal continuum subtraction is 7.9 pc cm⁻⁶. For NGC 300 the range is 4.6 – 7.9 pc cm⁻⁶, and the nominal value is 6.7 pc cm⁻⁶. A *cos i* correction was applied to NGC 300 and NGC 253, so these numbers indicate face-on surface brightness. This is probably an over-correction due to dust extinction in the disk, the vertical extent of the disk, and the DIG concentration in spiral arms. For NGC 55 we measured the average emission measure in a 20.24' \times 4.45' box centered on the galaxy in the masked image, parallel to the major axis. We then deprojected the observed average emission measure using a simple approximation of a uniformly-filled cylinder. The face-on average emission measure using this simple model is 8.5 – 11 pc cm⁻⁶. These values are lower limits to the true average surface brightness of the DIG, because the area considered is not completely filled with DIG. The average emission measure is certainly higher in the spiral arms. In the solar neighborhood the average emission measure of the DIG through the disk is 5.6 pc cm⁻⁶ (Reynolds 1984). In M31, WB94 find an average EM of 6 – 15 pc cm⁻⁶. Our values are consistent with these measurements.

Figure 6 shows the radial distribution of HII region and DIG emission for NGC 253 and NGC 300, corrected for inclination. The difference in the H α luminosity of these galaxies is apparent, especially in the nuclear region. The radial profiles show in a general sense the correlation of the DIG distribution with the HII region distribution. In the outer disks of

both galaxies, the DIG appears to contribute a larger portion of the total $H\alpha$ luminosity. Note that this effect occurs in the faintest part of the galaxy, where the emission measure is less than 10 pc cm^{-6} . This part of the galaxy is very sensitive to continuum subtraction errors, background errors, and flat-fielding errors, as can be seen by the error bars of figure 6. The loss of sensitivity in this region precludes us from claiming that the diffuse fraction varies with radius. Ferguson *et al.* (1996) have found an increase in the diffuse fraction with radius in one of the galaxies in their sample, NGC 7793. The inner and intermediate disks of NGC 300 and NGC 253, where the uncertainty is less, show a DIG contribution that is fairly constant.

The contribution of DIG to the total $H\alpha$ luminosity of these galaxies seems to be a constant fraction of the HII region luminosity, both within and among different galaxies. This and the noted correlation with star-forming regions implies a close correlation of massive stars with the DIG.

5. Spectral Properties of the DIG

In this section we investigate the $[SII]/(H\alpha+[NII])$ ratio of the DIG, which may help in constraining the ionization mechanism. We applied the mask (see §4) to both the $H\alpha$ and $[SII]$ images to compute the diffuse fractions in each line. The ratio of the resulting fluxes is shown in table 3. The same was done for HII region emission. These values were calculated after the correction for scattered light. The ratio in HII regions is about 0.2, while that measured in the DIG is about 0.35. The error bars indicate the variation due to continuum subtraction, and mostly reflect the sensitivity of the $[SII]$ emission to the continuum scale factor. The $[SII]$ luminosity of NGC 253 is extremely dependent on the continuum subtraction, varying by $\pm 55\%$ when the continuum is varied by $\pm 3\%$. Varying the continuum scale factor changed the $[SII]$ luminosity of NGC 55 and NGC 300 by $\pm 19\%$ and $\pm 35\%$, respectively, so this effect is less serious for these galaxies. Our measurements also contain some $[NII]$ emission. If the $[NII]/H\alpha$ ratio is also higher in the DIG, as some studies (Keppel *et al.* 1991; Dettmar & Schulz 1992) have indicated for NGC 891, then the actual difference in the $[SII]/H\alpha$ ratios is higher than our measurements indicate. For example, if the $[NII]/H\alpha$ ratio in the DIG were 0.6 (the value obtained by Dettmar & Schulz (1992) for a height of 0.5 kpc above the plane), compared to 0.3 in HII regions, the corrected $[SII]/H\alpha$ ratio for HII regions would be 0.26, but the ratio in the DIG would be 0.56. Dettmar & Schulz (1992) saw $[NII]/H\alpha$ ratios as high as 1.1 at $z=1$ kpc above the plane, further enhancing the difference. However, no increase in the $[NII]/H\alpha$ has been seen in the Galactic studies (Reynolds 1990).

To further investigate the line ratio in the DIG, we plot in figure 7 the intensity ratios of regions in the diffuse gas and in HII regions as a function of $H\alpha$ intensity for the Sculptor galaxies. Due to the near face-on orientation of NGC 300, emission measures up to 40 pc cm^{-6} in NGC 300 should be compared with emission measures up to 100 pc cm^{-6} in the inclined galaxies. The regions were measured in $9'' \times 9''$ boxes. The HII regions (figure 7 a-c) consistently show $[SII]/(H\alpha+[NII])$ ratios around 0.2, with small 1σ error bars. The diffuse gas (figure 7 d-f) shows a higher ratio, typically around 0.3 to 0.5. The error bars in each plot are a combination of photon noise and continuum subtraction variation. The large error bars for NGC 253 again reflect the sensitivity of the $[SII]$ luminosity to the amount of continuum subtracted in this galaxy. The ratio obtained for HII regions is contaminated by foreground DIG. This tends to overestimate the observed ratio, especially in faint HII regions.

Investigation of the ratios in individual boxes shows the change in the $[SII]/(H\alpha+[NII])$ ratio between HII regions and DIG. The high ratio is present in the diffuse layer around HII regions, in the inter-arm emission of the inner disk of NGC 253, and in the discrete structures such as the loops and shells in NGC 300 and NGC 55. The DIG projected within the shells shows the same spectral signature. In NGC 55 we note that the enhanced ratio exists in the diffuse emission above the plane of the galaxy. However, our images are not sensitive enough to tell if the ratio changes with height above the plane. There is a suggestion that the $[SII]/(H\alpha+[NII])$ ratio increases with distance from HII regions, but this result is not conclusive given the signal to noise ratio of the data and the systematic errors present. However, spectroscopy of the DIG in M31 has shown this effect (Greenawalt, Walterbos & Braun 1996).

For the Galaxy the $[SII]6716\text{\AA}/H\alpha$ ratio has been observed to vary from 0.07 to 0.18 in HII regions, with the higher ratio corresponding to the most dilute HII regions (Reynolds 1988). The observed ratios for DIG (or Warm Ionized Medium) in the Galaxy are 0.3 to 0.5 (Reynolds 1985) corresponding to a $[SII]6716+6731\text{\AA}/H\alpha+[NII]6548+6583\text{\AA}$ ratio of 0.35 to 0.57. The trend for higher $[SII]/H\alpha$ ratios has also been seen in the DIG of other galaxies such as M31 (WB94) and M51 and M81 (Greenawalt & Walterbos 1996). Our results for the Sculptor galaxies are consistent with those reported previously. The high $[SII]/H\alpha$ ratio can occur in a shock ionized environment, suggesting that shocks from supernovae may be an important ionization source. However, the ratio is critically dependent on the shock velocity (Mathis 1986). Overall, the $[SII]/H\alpha$ ratio seems to be rather constant in the DIG, which would seem to indicate an unrealistically constant shock speed (Mathis 1986). In addition, the energy requirement of the DIG in several galaxies is higher than can be provided by supernovae (WB94; Rand *et al.* 1990). Photoionization in a diffuse medium (Mathis 1986) can also produce the observed ratio, with perhaps a contribution

from photoelectric heating by dust grains (Reynolds & Cox 1992; Sivan *et al.* 1986). If photoionization is the mechanism responsible for the DIG, the structure of the ISM, and particularly of neutral Hydrogen, must be better understood to make it clear how ionizing photons can travel the large distances required to reach the DIG without being absorbed.

6. Summary and Discussion

The data presented in the preceding sections show the presence of DIG in NGC 55, NGC 253, and NGC 300. The contribution of DIG emission to the total $H\alpha$ luminosity is observed to be 33 to 58% in all three galaxies, uncorrected for extinction. After correcting for scattered light, the diffuse fraction is between 30 and 54%. The average emission measure of the two non-edge-on galaxies is 6.2 pc cm^{-6} for NGC 300 and 6.6 pc cm^{-6} for NGC 253. The diffuse emission is strongest near HII regions and in the inner disks of these galaxies, and is observed both as a diffuse layer and with filamentary structure in the form of shells and loops. The global distribution of DIG in the disks seems to be correlated with the HII region distribution, implying a connection with star formation. The $[SII]/(H\alpha + [NII])$ ratio is enhanced in the DIG compared to HII regions, with ratios of 0.3-0.5, compared to around 0.2 for HII regions. All of the derived characteristics compare well with the values seen in the Milky Way and in other spirals galaxies.

One of the surprising discoveries about the DIG in spiral galaxies is the constancy of the fraction of the total $H\alpha$ luminosity of a galaxy that it contributes. WB94 measured 40% for M31, and all results obtained since have come up with a similar number: for the galaxies studied here, we find fractions between 30 and 54%, for M51 and M81 we find 30 to 40% (Greenawalt & Walterbos 1996), while Ferguson *et al.* (1996) find 53% for NGC 247 and 41% for NGC 7793. If it were not for the difference in $[SII]$ over $H\alpha$ intensity ratio in the DIG compared to HII regions, we might in fact question whether we are mostly detecting $H\alpha$ photons that were scattered into the line of sight by dust grains, but originally came from the HII regions. But given the $[SII]$ data that seems unlikely, although it may be worthwhile to model this more accurately to place some limits on a possible scattered light contribution. The $[SII]$ data also make it unlikely that the DIG is a collection of faint unresolved HII regions. The HII region luminosity function of Kennicutt *et al.* (1989) suggests that no more than 5% of the DIG emission in the Sculptor galaxies studied here can arise in unresolved HII regions.

The constancy of the diffuse fraction is surprising because of the differences that exist in Hubble type and star formation activity of the galaxies studied; quiescent spirals (M81 and M31), a vigorously star forming Sbc (M51), a late-type Sd (NGC 300), and a

starburst (NGC 253). An understanding of this situation cannot be reached without better knowledge of the source of ionization of the DIG. The high fractional H α luminosity for the DIG almost certainly implies that *photoionization* has to dominate, but which stellar types dominate? The close association between DIG and HII regions makes it tempting to think in terms of Ly γ photons leaking from HII regions. However, there is not yet independent evidence to support this, and the lack of Ly γ photons leaking from relatively unobscured starburst nuclei (Leitherer *et al.* 1995) would perhaps indicate that such leakage may not be very likely. The close association between DIG and HII regions would, for example, also be expected if the DIG is mostly ionized by field OB stars which are no longer associated with discrete HII regions. Whether such stars can produce the required Ly γ photon rates needs to be determined from a careful census of such stars in specific regions; we are not aware that any such studies have been done for the galaxies in which the DIG has been analyzed. A recent attempt was made by Patel & Wilson (1995a & b), however, without having accurate data on the spectral types of the stars. We are now working on several approaches. Nevertheless, in any case the constancy of DIG fractional H α luminosities appears remarkable.

We appreciate the help of the CTIO staff, in particular Bill Weller, during the CTIO observing run. We acknowledge useful discussions with Rob Kennicutt and Vanessa Galarza. This research was supported by the NSF through grant AST-9123777, and by a Cottrell Scholarship Award from Research Corporation. BEG was supported by a grant from the New Mexico Space Grant Consortium.

REFERENCES

- Alcaino, G., & Liller, W. 1984, AJ, 89, 814
Burstein, D., & Heiles, C. 1984, ApJS, 54, 33
Dettmar, R.-J. 1990, A&A, 232, L15
Dettmar, R.-J., & Schulz, H. 1992, A&A, 254, L25
Ferguson, A. M. N., Wyse, R. F. G., Gallagher, J. S., & Hunter, D. A. 1996, AJ, 111, 2265
Graham, J. A. & Lowrie, D. G. 1982, ApJ, 253, L73
Greenawalt, B. E., & Walterbos, R. A. M., 1996, to be submitted to ApJ
Greenawalt, B. E., Walterbos, R. A. M., & Braun, R. 1996, submitted to ApJ Letters
Hamuy, M., Walker, A. R., Suntzeff, N. B., Gigoux, P., Heathcote, S. R., & Phillips, M. M. 1992, PASP, 104, 533

- Heckman, T. M., Armus, L., & Miley, G. K. 1990, *ApJS*, 74, 833
- Hester, J. J., & Kulkarni, S. R. 1990, in *The Interstellar Medium in External Galaxies*, ed D. Hollenbach & H. Thronsen (NASA CP-3084), 288
- Hunter, D. A., & Gallagher, J. S. 1990, *ApJ*, 362, 480
- Keel, W. C. 1984, *ApJ*, 282,75
- Kennicutt, R. C. 1983, *ApJ*, 272, 54
- Kennicutt, R. C. 1992, *ApJ*, 388, 310
- Kennicutt, R. C., Edgar, B. K., & Hodge, P. W. 1989, *ApJ*, 337, 761.
- Keppel, J. W., Dettmar, R. J., Gallagher, J. S., & Roberts, M. S. 1991, *ApJ*, 374, 507
- Kulkarni, S. R., & Heiles, C. E. 1988, in *Galactic and Extragalactic Radio Astronomy*, ed. G. L. Verschuur & K. I. Kellerman (New York: Springer), 95
- Leitherer, C., Ferguson, H. C., Heckman, T. M., Lowenthal, J. D., 1995, *ApJ*, 454, L19
- Mathis, J. S. 1986, *ApJ*, 301,423
- Patel, K. & Wilson, C. D. 1995a, *ApJ*, 451, 607
- Patel, K. & Wilson, C. D. 1995b, *ApJ*, 453, 162
- Pence, W. D. 1981, *ApJ*, 247, 473
- Puche, D., & Carignan, C. 1988, *AJ*, 95, 1025
- Rand, R. J., Kulkarni, S. R. & Hester, J. J. 1990, *ApJ*, 352, 1
- Reynolds, R. J. 1984, *ApJ*, 282, 191
- Reynolds, R. J. 1985, *ApJ*, 294, 256
- Reynolds, R. J. 1988, *ApJ*, 333, 341
- Reynolds, R. J. 1990, in *IAU Symposium 139, The Galactic and Extragalactic Background Radiation*, ed S. Bowyer, & C. Leinert (Dordrecht:Kluwer), 157
- Reynolds, R. J. 1991, in *IAU Symposium 144, The Interstellar Disk-Halo Connection in Galaxies*, ed H. Bloemen (Dordrecht:Kluwer), 67
- Reynolds, R. J. & Cox, D. P. 1992, *ApJ*, 400, L33
- Rice, W., Longsdale, C. J., Soifer, B. T., Neugebauer, G., Koplan, E. L., Lloyd, L. A., DeJong, T., Habing, H. J. 1988, *ApJS*, 68, 91
- Sandage, A. 1961, *The Hubble Atlas of Galaxies* (Washington: Carnegie Institution), 34
- Schulz, H., & Wegner, G. 1992, *A&A*, 266, 167

- Sivan, J.-P., Stasinska, G., & Lequeux, J. 1986, *A&A*, 158, 279
- Sivan, J.-P., Petit, H., Conti, G. & Maucherat, A. J. 1990, *A&A*, 237, 23
- Smith, B. J. & Harvey, P. M. 1996 Preprint
- Sofue, Y., Wakamatsu, K., & Malin, D. F. 1994, *AJ*, 108, 2102
- Tully, R. B. 1988, *Nearby Galaxies Catalog* (Cambridge: Cambridge University Press)
- Walterbos, R. A. M., & Braun, R. 1992, *A&AS*, 92, 625
- Walterbos, R. A. M., & Braun, R. 1994 (WB94), *ApJ*, 431, 156

Fig. 1.— The continuum subtracted $H\alpha$ image of NGC 55. This and the following images have been multiplied by $\cos i$ to put them on a uniform brightness scale. The inclination of NGC 55 is 90° , however, so the same correction used for NGC 253 ($i=78.5^\circ$) was used here. The image is scaled logarithmically to enhance the faintest emission levels. The greyscale ranges from -2 to 500 pc cm^{-6} . We added a constant to the image so that the entire range was positive, to enable the logarithmic scaling. The bar at the lower left corresponds to 1 kpc at the distance of NGC 55. North is 18° clockwise from the top and East is 90° counter-clockwise from North. The diagonal pattern is a result of bias structure on the chip (see §2.2).

Fig. 2.— The continuum subtracted $H\alpha$ image of NGC 253, scaled to face-on by multiplying the intensities with $\cos i$. The circle near the southwest side of the galaxy corresponds to a poorly subtracted bright star that was edited out. The levels vary from -2 to 500 pc cm^{-6} . The bar at the lower left corresponds to 1 kpc at the distance of NGC 253. The image has been rotated so that North is 52° counter-clockwise from the top, and East is 90° counter-clockwise from North.

Fig. 3.— The continuum subtracted $H\alpha$ image of NGC 300, scaled to face-on by multiplying the intensities with $\cos i$. The levels vary from -6 to 500 pc cm^{-6} . The lower value was chosen to keep the noise at the same grey levels as for the inclined galaxies, which were scaled differently due to the $\cos i$ correction. The bar at the lower left corresponds to 1 kpc at the distance of NGC 300. North is up and East is on the left.

Fig. 4.— (a) A masked image of NGC 253, using a cut at a constant isophote of 80 pc cm^{-6} . The black areas on the galaxy are regions that the masking technique defines as HII regions, where the pixel value has been replaced by zero. This mask completely removes the inner disk, even though significant diffuse emission is seen there in figure 2. (b) This masked image was made using the median-subtracted image method (see text §4.2). This mask is much better at differentiating between the HII regions and DIG on the basis of surface brightness, because the variation of the background DIG has been removed in the masking process.

Fig. 5.— Comparison of the effect of different isophotal cut-off levels used in masking HII regions on the DIG fractional $H\alpha + [\text{NII}]$ luminosity. These curves correspond to the case where no median filtering was used (c.f. figure 4a). The dashed lines show the variation with continuum subtraction. At lower cut-off levels, the diffuse fractions are comparable to those measured for the Milky Way. Thus the relative power requirements of the DIG may well be similar for the Sculptor galaxies and the Milky Way.

Fig. 6.— Radial profiles of $H\alpha + [\text{NII}]$ emission for NGC 253 and NGC 300. The surface brightness is given in emission measure. Note the difference in scale on the y-axis. Error

bars are estimated from the background uncertainty due to flat fielding errors. Averaging azimuthally should reduce the uncertainty by at least a factor of two, so the error bars here indicate half those that would result from the estimated flat field uncertainty.

Fig. 7.— The $[SII]/(H\alpha + [NII])$ ratio for selected regions in the Sculptor galaxies. Each point is the ratio in a $9'' \times 9''$ box. In (a)-(c) (NGC 55, NGC 253, and NGC 300, respectively) each box contains (part of) an HII region, and in (d)-(f) the boxes are placed in the DIG. The solid line is the mean of all the points in bins of 200 pc cm^{-6} for HII regions and 10 pc cm^{-6} for DIG. Representative error bars on the mean are shown in each plot. They are a combination of rms error measured in the background plus uncertainty due to the continuum subtraction. These are observed values and are inclination dependent, which has no effect on the ratio but does mean that the lower range of $H\alpha + [NII]$ emission measure for NGC 300 (up to 40 pc cm^{-6}) should be compared with the entire range (up to 150 pc cm^{-6}) for the inclined galaxies. This is why there are no points at higher emission levels in the DIG in NGC 300.